


PSFC/JA-00-20

Confinement Criterion for a Highly Bunched Beam

View metadata, citation and similar papers at core.ac.uk

brought to you by  C
provided by DSpace

M. Hess and C. Chen

July, 2000

Plasma Science and Fusion Center
Massachusetts Institute of Technology
Cambridge, MA 02139, USA

This work was supported by the Air Force Office of Scientific Research, Grant No. F49620-97-1-0480 and Grant No. F49620-00-1-0007 and by the Department of Energy, Office of High-Energy and Nuclear Physics, Grant No. DE-FG02-95ER-40919. Reproduction, translation, publication, use and disposal, in whole or part, by or for the United States government is permitted.

Submitted for publication in *Physics of Plasmas*.

CONFINEMENT CRITERION FOR A HIGHLY BUNCHED BEAM

Mark Hess and Chiping Chen
Plasma Science and Fusion Center
Massachusetts Institute of Technology
Cambridge, MA 02139

ABSTRACT

The non-relativistic motion is analyzed for a highly bunched beam propagating through a perfectly conducting cylindrical pipe confined radially by a constant magnetic field parallel to the conductor axis. In the present analysis, the beam is treated as either a thin rod distribution representing a continuous (unbunched) beam or periodic collinear point charges representing a highly bunched beam. Use is made of a Green's function to compute the electrostatic force on the beam due to the induced surface charge in the conductor wall. By analyzing the Hamiltonian dynamics, a criterion is derived for the confinement of unbunched and bunched beams. It is shown that for the confinement of beams with the same charge per unit length, the maximum value of the effective self-field parameter is $2\mathbf{w}_p^2/\mathbf{w}_c^2 \cong 2a/L$ for a highly bunched beam with $a \ll L$. This value is significantly lower than the Brillouin density limit for an unbunched beam $2\mathbf{w}_p^2/\mathbf{w}_c^2 = 1$. Here a is the radius of the conducting cylinder, and L is the periodic spacing of the bunches.

PACS: 29.27, 41.85

I. Introduction

Confinement and transport of high-intensity charged-particle beams are important subjects in both plasma physics and beam physics^{1,2}. It is well known that for a continuous, non-neutral, charged-particle beam propagating in a uniform magnetic field, the maximum beam density is determined by the so-called Brillouin density limit^{3,4}. For nonrelativistic beams, the Brillouin density limit corresponds to the condition

$2\mathbf{w}_p^2/\mathbf{w}_c^2 = 1$, where $\mathbf{w}_p = (4\pi q^2 n/m)^{1/2}$ is the nonrelativistic plasma frequency, and $\mathbf{w}_c = qB/mc$ is the nonrelativistic cyclotron frequency. Although there is a large body of literature on the equilibrium and stability properties of high-intensity continuous non-neutral charged-particle beams, high-intensity bunched beams are rarely discussed in the literature⁵⁻⁷.

There is a need to gain a fundamental understanding of high-intensity bunched beams because they are widely employed in high-power microwave (HPM) sources, such as klystrons and traveling wave tubes, as well as in high-intensity particle accelerators such as high-intensity linacs. In both HPM sources and high-intensity particle accelerators, an important problem associated with lack of full beam confinement caused by the bunching of the electron and ion beam in the direction of beam propagation is beam loss, through such mechanisms as beam halo formation⁸⁻¹⁰.

In this paper, we analyze the nonrelativistic motion of a highly bunched beam propagating through a perfectly conducting cylindrical pipe confined radially by a constant magnetic field parallel to the conductor axis. In the present analysis, the beam is treated as either a thin rod distribution representing a continuous (unbunched) beam or periodic collinear point charges representing a highly bunched beam. Use is made of the

Green's function to compute the electrostatic force on the beam due to the induced surface charge in the conductor wall. From Hamilton's equations, the radial phase space is studied for both unbunched and bunched beams. In general, the radial phase space contains both closed orbits (i.e., trapped particle orbits) and untrapped orbits (i.e., orbits which intersect the conductor wall) at sufficiently low beam densities, whereas only untrapped orbits exist at sufficiently high beam densities. By determining the conditions for the disappearance of trapped particle orbits, a criterion for the confinement of a highly bunched beam is derived. It is shown that for the confinement of beams with the same charge per unit length, the maximum value of the effective self-field parameter is $2w_p^2/w_c^2 \cong 2a/L$ for a highly bunched beam with $a \ll L$, where a is the radius of the conducting cylinder and L is the periodic spacing of the bunches. This result is significantly lower than the Brillouin density limit $2w_p^2/w_c^2 = 1$ for an unbunched beam.

The paper is organized as follows. In Sec. II, a Green's function model is presented for unbunched and bunched beams, and the electrostatic field produced by the induced surface charge is computed. In Sec. III, the Hamiltonian dynamics of the beam is studied. In Sec. IV, a criterion is derived for the confinement of unbunched and bunched beams. Discussions and conclusions are in Sec. V and VI, respectively.

II. Green's Function Description of Space Charge

The systems we are analyzing consist of periodic space charge in an infinite perfectly conducting cylinder, which is grounded, as shown in Fig. 1. In particular, we investigate the dynamics of two types of periodic space charge. One type is a uniform rod of charge, shown in Fig. 1(a) representing an unbunched beam. Another type is a collinear distribution of charges equally spaced by a distance, L , shown in Fig. 1(b) representing a highly bunched beam. The radius of the cylinder is a , and the distance from the axis that the space charge is displaced is r . We assume that there exists an applied uniform magnetic field $\vec{B} = B \hat{e}_z$, and \hat{e}_z denotes the unit vector parallel to the axis of the conductor. Physically the 2-D case is recovered from the 3-D case by taking the limit $a/L \rightarrow \infty$ for a fixed charge density.

The presence of the periodic space charge induces a charge density, \mathbf{s} , on the surface of the conductor. The induced surface charge provides an electrostatic force on the space charge. We assume that the transverse velocity of the space charge is sufficiently small compared to the speed of light, hence only the electrostatic force from the conducting wall and the applied magnetic force are non-negligible in the system.

In order to compute the induced surface charge and the electrostatic force, we first formulate a Green's function, which is the electrostatic potential inside the entire cylinder for a given distribution of unit charge(s). In cgs units, the Green's function, G , satisfies the Laplace's equation,

$$\nabla^2 G = -4\pi \delta(\vec{x} - \vec{x}') \quad (1)$$

where the primed coordinates denote the position of the charge(s) and the unprimed coordinates denote the point of observation. For the 2-D rod of charge,

$$r(\bar{x} - \bar{x}') = \frac{1}{r} \mathbf{d}(r - r') \mathbf{d}(q - q') \quad (2)$$

while for the 3-D collinear distribution,

$$r(\bar{x} - \bar{x}') = \frac{1}{r} \mathbf{d}(r - r') \mathbf{d}(q - q') \sum_{n=-\infty}^{\infty} \mathbf{d}(z - z' - nL) \quad (3)$$

where $\mathbf{d}(x)$ is the Dirac \mathbf{d} -function.

The Green's function for both distributions satisfies three other criteria; it must be both rotationally invariant by $2\mathbf{p}$ and translationally invariant by nL in the unprimed coordinates, and the function must be zero at the conductor (Dirichlet condition), i.e.

$$\begin{aligned} G|_{q+2\mathbf{p}} &= G|_q \\ G|_{z+nL} &= G|_z \\ G|_{r=a} &= 0 \end{aligned} \quad (4)$$

A solution to (1) can be formed by expanding in terms of eigenfunctions of Laplace's equation in cylindrical coordinates. For the 3-D case, we find the solution ^{11, 12}

$$G_{3D} = \frac{2}{L} \sum_{n=-\infty}^{\infty} \sum_{l=-\infty}^{\infty} e^{in(\hat{z} - \hat{z}')} e^{il(q - q')} \frac{I_l(n\hat{r}_{<})}{I_l(na)} \left[I_l(na) K_l(n\hat{r}_{>}) - I_l(n\hat{r}_{>}) K_l(na) \right], \quad (5)$$

where

$$\hat{r} = \frac{2pr}{L}, \quad \hat{r}' = \frac{2pr'}{L}, \quad \hat{z} = \frac{2pz}{L}, \quad \hat{z}' = \frac{2pz'}{L}, \quad a = \frac{2pa}{L}, \quad (6)$$

and the notation $\hat{r}_{>|<}$ represents the greater(lesser) of \hat{r} and \hat{r}' . Simplification of (5) is possible by summing over the $n = 0$ terms, and combining the $n < 0$ terms with their positive counterparts yielding,

$$\begin{aligned}
G_{3D} = & \frac{1}{L} G_{2D} + \frac{4}{L} \sum_{n=1}^{\infty} \cos[n(\hat{z} - \hat{z}')] \frac{I_0(\hat{r}_<)}{I_0(\hat{r}_>)} \left[I_0(\hat{r}_<) K_0(\hat{r}_>) - I_0(\hat{r}_>) K_0(\hat{r}_<) \right] \\
& + \frac{8}{L} \sum_{n=1}^{\infty} \sum_{l=1}^{\infty} \cos[n(\hat{z} - \hat{z}')] \cos[l(\mathbf{q} - \mathbf{q}')] \frac{I_l(\hat{r}_<)}{I_l(\hat{r}_>)} \left[I_l(\hat{r}_<) K_l(\hat{r}_>) - I_l(\hat{r}_>) K_l(\hat{r}_<) \right]
\end{aligned} \quad (7)$$

where G_{2D} represents the solution of (1) for the 2-D rod distribution. G_{2D} is given by

$$G_{2D} = \ln \left| \frac{\mathbf{a}^2 + \hat{r}_> \hat{r}_< / \mathbf{a}^2 - 2\hat{r}_> \hat{r}_< \cos(\mathbf{q} - \mathbf{q}')}{\hat{r}_>^2 + \hat{r}_<^2 - 2\hat{r}_> \hat{r}_< \cos(\mathbf{q} - \mathbf{q}')} \right| \quad (8)$$

which is well known¹³.

Since the Green's function represents the electrostatic potential of a unit charge, we can readily calculate the electric field at the surface of the wall and the induced surface charge density, \mathbf{s} , using the relation

$$\mathbf{s} = \frac{\hat{n} \cdot \vec{E}|_{\text{surface}}}{4\mathbf{p}} = \frac{-C\hat{n} \cdot \vec{\nabla}G|_{\text{surface}}}{4\mathbf{p}} = \frac{C}{2L} \frac{\partial G}{\partial \hat{r}} \Big|_{\hat{r}=\mathbf{a}}, \quad (9)$$

where \hat{n} denotes the unit vector perpendicular to the surface ($\hat{n} = -\hat{e}_r$) and \vec{E} is the electric field. C is a factor which depends on whether we are solving the 2-D or 3-D problem. For the 3-D problem, C is equal to q , the value of each individual charge. For the 2-D problem, C is equal to I , the charge per unit length of the rod.

For the 2-D case, the induced surface charge density is

$$\mathbf{s}_{2D} = -\frac{I}{La} \left| \frac{\mathbf{a}^2 - \hat{r}'^2}{\mathbf{a}^2 + \hat{r}'^2 - 2\mathbf{a}\hat{r}' \cos(\mathbf{q} - \mathbf{q}')} \right| = -\frac{I}{La} \hat{\mathbf{s}}_{2D}, \quad (10)$$

while for the 3-D case we have,

$$\begin{aligned}
\mathbf{s}_{3D} = & -\frac{\hat{\mathbf{s}}_{2D}}{L^2 \mathbf{a}} - \frac{2}{L^2 \mathbf{a}} \sum_{n=1}^{\infty} \cos[n(\hat{z} - \hat{z}')] \frac{I_0(\hat{r}')}{I_0(\hat{r}_>)} \\
& - \frac{4}{L^2 \mathbf{a}} \sum_{n=1}^{\infty} \sum_{l=1}^{\infty} \cos[n(\hat{z} - \hat{z}')] \cos[l(\mathbf{q} - \mathbf{q}')] \frac{I_l(\hat{r}')}{I_l(\hat{r}_>)}
\end{aligned} \quad (11)$$

In deriving (11), use has been made of the Wronskian, $I_1 \partial_x (K_1 \partial_x \psi) - I_1' \partial_x (K_1' \partial_x \psi) = -1/x$.

We are now in a position to compute the electric field, \vec{E}^{self} , which is exerted on the charge distribution inside the conductor by the induced surface charge. Because of the system's symmetry in the \hat{e}_ϕ and \hat{e}_z directions, the electric field at the charge distribution can only be in the \hat{e}_r direction. Since the sign of the surface charge is opposite to that of the internal charges, the force must be attractive. \vec{E}^{self} can be obtained by integrating the differential electric field vector, evaluated at the charge distribution location, over the entire conductor,

$$\vec{E}^{self}(\vec{r}') = \int_{surface} dS \frac{(\vec{r}' - \vec{r}_s) \rho(\vec{r}_s)}{|\vec{r}' - \vec{r}_s|^3}. \quad (12)$$

\vec{r}_s is the vector measured from the central axis of the conductor to the point of the differential charge. As will be demonstrated in the Appendix,

$$\vec{E}_{2D}^{self}(\vec{r}') = \frac{4\pi l}{L} \left(\frac{\hat{r}'}{a^2 - \hat{r}'^2} \right) \hat{e}_{r'}, \quad (13)$$

for the 2-D case, and

$$\begin{aligned} \vec{E}_{3D}^{self}(\vec{r}') &= E_{3D}^{self} \hat{e}_{r'}, \\ E_{3D}^{self} &= \frac{4\pi q}{L^2} \left(\frac{\hat{r}'}{a^2 - \hat{r}'^2} \right) + \frac{8\pi q}{L^2} \sum_{n=1}^{\infty} \frac{n I_0(\hat{r}') I_0'(\hat{r}') K_0(na)}{I_0(na)} \\ &\quad + \frac{16\pi q}{L^2} \sum_{n=1}^{\infty} \sum_{l=1}^{\infty} \frac{n I_l(\hat{r}') I_l'(\hat{r}') K_l(na)}{I_l(na)} \end{aligned} \quad (14)$$

for the 3-D system.

III. Hamiltonian Dynamics

We can investigate the radial dynamics of one rod of charge (2-D) or one string of charges (3-D) interacting with its self-field (14) and a constant applied magnetic field, $\vec{B} = B \hat{e}_z$. In this system, there are no forces in the longitudinal direction. Therefore we may describe all of the dynamics using a Hamiltonian in the radial and azimuthal directions and set $v_z = 0$ without loss of generality. In particular, the Hamiltonian for transverse motion is given by,

$$H = \frac{1}{2m} \left[P_r - \frac{qA_r}{c} \right]^2 + \frac{1}{r^2} \left[P_q - \frac{rqA_q}{c} \right]^2 + q\mathbf{f}^{self} \quad (15)$$

where \vec{P} is the canonical momentum, $\vec{A} = \frac{rB}{2} \hat{e}_\phi$ is the vector potential, and

$$\mathbf{f}^{self} = - \int_0^r E^{self} dr \quad (16)$$

For the 2-D system, we can set $m = \mathbf{r} L$ where \mathbf{r} is the mass density of the rod, and $q = \mathbf{I} L$. Dividing by L on both sides of (15) yields a Hamiltonian per unit length, which correctly describes the 2-D dynamics. Applying Hamilton's equations to (15), gives the following set of normalized equations:

$$\begin{aligned} \frac{d\hat{r}}{dt} &= \hat{P}_r & , & & \frac{d\hat{P}_r}{dt} &= \frac{\hat{P}_q^2}{\hat{r}^3} - \hat{r} + \mathbf{x} \hat{E}^{self} \\ \frac{d\hat{q}}{dt} &= \frac{\hat{P}_q}{\hat{r}^2} - 1 & , & & \frac{d\hat{P}_q}{dt} &= 0 \end{aligned} \quad (17)$$

where normalized variables and parameters are defined by

$$\begin{aligned}
\mathbf{t} &= \mathbf{w}_L t, \quad \hat{P}_r = \frac{2\mathbf{p}P_r}{mL\mathbf{w}_L}, \quad \hat{P}_q = \left[\frac{2\mathbf{p}}{L} \right]^2 \frac{P_q}{m\mathbf{w}_L} \\
\hat{E}^{self} &= \frac{L^2 E^{self}}{4\mathbf{p}q}, \quad \mathbf{x} = \frac{32\mathbf{p}^2 mc^2}{L^3 B^2}, \quad \mathbf{w}_L = \frac{qB}{2mc}
\end{aligned} \tag{18}$$

and \mathbf{w}_L represents the Larmor frequency. From (17), it is obvious that the canonical angular momentum is conserved. Combining the first two equations in (17), and denoting initial conditions with a subscript 0, we can find an expression relating the canonical radial momentum with the radial position,

$$\hat{P}_r = \pm \sqrt{\hat{P}_{r0}^2 + F(\hat{r}_0) - F(\hat{r})} \tag{19}$$

where F represents an effective potential energy, and is given by,

$$F(\hat{r}) = \frac{\hat{P}_q^2}{\hat{r}^2} + \hat{r}^2 + \mathbf{x} \ln \left| 1 - \frac{\hat{r}^2}{\mathbf{a}^2} \right| \tag{20}$$

for the 2-D case while

$$F(\hat{r}) = \frac{\hat{P}_q^2}{\hat{r}^2} + \hat{r}^2 + \mathbf{x} \ln \left| 1 - \frac{\hat{r}^2}{\mathbf{a}^2} \right| - 2\mathbf{x} \sum_{n=1}^{\infty} \frac{K_0(n\mathbf{a})}{I_0(n\mathbf{a})} I_0^2(n\hat{r}) - 4\mathbf{x} \sum_{n=1}^{\infty} \sum_{l=1}^{\infty} \frac{K_l(n\mathbf{a})}{I_l(n\mathbf{a})} I_l^2(n\hat{r}) \tag{21}$$

for the 3-D case. Making use of the asymptotic properties of the modified Bessel functions, it is readily shown that in the limit $a/L \rightarrow \infty$, $F(\hat{r})$ in (21) for the 3-D case approaches to $F(\hat{r})$ in (20) for the 2-D case. Therefore, the analysis of confinement in the 2-D system will be fully recovered in the 3-D analysis in the $a/L = \infty$ limit.

Figures 2(a) and 2(b) show $F(\hat{r})$ plotted for two different sets of values of (\mathbf{x}, \hat{P}_q) for the 2-D system. There are two possible behaviors for this function to have. In Fig. 2(a), there is a kink (i.e. the function has one local minimum and one local maximum), while for Fig. 2(b) the function is monotonically decreasing. A function, $F(\hat{r})$, with a kink

leads to a radial phase space (\hat{r}, \hat{P}_r) , as is illustrated in Fig. 3(a), which contains both trapped and untrapped particle orbits. An untrapped particle orbit will result in the particle eventually being lost to the conductor wall, whereas a trapped orbit corresponds to a particle confined inside of the perfectly conducting cylinder. A monotonically decreasing function as in Fig. 2(b), will produce a phase space such as Fig. 3(b), which only contains untrapped particle orbits.

To illustrate the 3-D effects (i.e. effects of beam bunching), we compare the phase space for the 3-D case in Figs. 4(a) and 4(b) with the 2-D case shown in Fig. 3. In particular, 4(a), which has only untrapped orbits, has the same \mathbf{x} and \hat{P}_q values as 3(a), illustrating the added effect of the electric field in the 3-D regime. However, trapped particle orbits do exist at lower values of \mathbf{x} such as for the value of \mathbf{x} shown in Fig. 4(a).

IV. Conditions for Confinement

The complete criterion for trapped particle orbits is threefold, a) $F(\hat{r})$ must have a kink, b) the initial particle radius must be chosen between the local maximum of $F(\hat{r})$ and the other point on $F(\hat{r})$ corresponding to the same value, and c) the initial radial momentum must be sufficiently small, such that

$$\hat{P}_{r0}^2 \leq F(\hat{r}_0) - F(\hat{r})_{\min}. \quad (22)$$

The most important of the three criteria for trapped particle orbits is the first. We therefore determine the region in parameter space $\{\mathbf{a}, \mathbf{x}, \hat{P}_q\}$ space for both the 2-D and 3-D systems, such that $F(\hat{r})$ has a kink. In order to find this criterion for $F(\hat{r})$, i.e. that trapped particle orbits may exist, we must look for the conditions such that

$F'(\hat{r}) = F''(\hat{r}) = 0$, where $F'(\hat{r}) = dF(\hat{r})/d\hat{r}$ and $F''(\hat{r}) = d^2F(\hat{r})/d\hat{r}^2$. This represents that transition point between $F(\hat{r})$ being monotonic and non-monotonic.

A. Confinement for the 2-D System

It is evident in (20) that the only increasing term in $F(\hat{r})$ is the \hat{r}^2 term and all other terms are decreasing. When $\mathbf{x} = 0$, applying the transition condition $F'(\hat{r}) = F''(\hat{r}) = 0$ yields $|\hat{P}_q| = \mathbf{a}^2$ at $\hat{r} = \mathbf{a}$ for both systems. However, when $\hat{P}_q = 0$, it follows from (20) that $F(\hat{r}) = \hat{r}^2 + \mathbf{x} \ln[1 - \hat{r}^2/\mathbf{a}^2]$. Expanding $F(\hat{r})$ near $\hat{r} = 0$ yields $F(\hat{r}) \cong \hat{r}^2(1 - \mathbf{x}/\mathbf{a}^2)$. So $F(\hat{r})$ will not be monotonic at $\hat{r} = 0$ for sufficiently small \hat{P}_q when the coefficient of

the quadratic term is positive (i.e. when $\mathbf{x}/\mathbf{a}^2 < 1$). Therefore, the necessary conditions for $F(\hat{r})$ to have a kink are $|\hat{P}_q| < \mathbf{a}^2$ and $\mathbf{x}/\mathbf{a}^2 < 1$.

Manipulating the equation $F'(\hat{r}) = 0$ and letting $y = \mathbf{a}\hat{r}$, we find that

$$y^6 + (\mathbf{n} - 1)y^4 + (1 - y^2)\mathbf{m}^2 = 0, \quad (23)$$

where $\mathbf{m} = \hat{P}_q/\mathbf{a}^2$ and $\mathbf{n} = \mathbf{x}/\mathbf{a}^2$. Because $0 < y < 1$ ($0 < \hat{r} < \mathbf{a}$), we can further simplify (23) by letting $z = y^2$, and obtain

$$G(z) \equiv z^3 + (\mathbf{n} - 1)z^2 + (1 - z)\mathbf{m}^2 = 0, \quad (24)$$

where $0 < z < 1$. Note that $G(0) = \mathbf{m}^2 > 0$ and $G(1) = \mathbf{x} > 0$.

It is straightforward to show that $G(z)$ has precisely one zero when the transition point occurs. This statement is equivalent to stating that the minimum of $G(z)$ must be equal to zero, and that the minimum must occur between 0 and 1 for trapping to occur. These conditions yield

$$3z_{\min}^2 + 2(\mathbf{n} - 1)z_{\min} - \mathbf{m}^2 = 0, \quad (25)$$

$$0 < z_{\min} = \frac{(\mathbf{n} - 1) + \sqrt{(\mathbf{n} - 1)^2 + 3\mathbf{m}^2}}{3} < 1, \quad (26)$$

$$z_{\min}^3 + (\mathbf{n} - 1)z_{\min}^2 + (1 - z_{\min})\mathbf{m}^2 = 0 \quad (27)$$

where z_{\min} is the minimum of G .

Substituting (26) into (27) and solving for \mathbf{m} with the aid of (25) yields two possible solutions,

$$\mathbf{m}^2 = \mathbf{m}_+^2, \quad \mathbf{m}^2 = \mathbf{m}_-^2 \quad (28)$$

where

$$8\mathbf{m}_{\pm}^2 = 27 - 18|1 - \mathbf{n}_q - |1 - \mathbf{n}_q|^2 \pm \sqrt{(27 - 18|1 - \mathbf{n}_q - |1 - \mathbf{n}_q|^2)^2 - 64|1 - \mathbf{n}_q|^3}. \quad (29)$$

However, the inequality (26) yields, $\mathbf{m}^2 < 2\mathbf{n} + 1$, and by graphical inspection only $\mathbf{m}^2 < \mathbf{m}_{\pm}^2$ is possible. We find that for the 2-D system, the following inequality must be satisfied for trapped particle orbits to occur,

$$8\mathbf{m}^2 \leq 27 - 18|1 - \mathbf{n}_q - |1 - \mathbf{n}_q|^2 - \sqrt{(27 - 18|1 - \mathbf{n}_q - |1 - \mathbf{n}_q|^2)^2 - 64|1 - \mathbf{n}_q|^3} \quad (30)$$

Note that since \mathbf{m} and \mathbf{n} are both independent of L , (30) is also independent of L . Equation (30) is plotted later in Fig. 5 in terms of normalized P_q and the effective plasma frequency, as we compare the 2-D case with the 3-D case.

Since the effective density of particles for both systems is given by $n = (pa^2L)^{-1}$, we can relate \mathbf{x}/\mathbf{a}^2 to the effective plasma frequency $\mathbf{w}_p = (4\mathbf{p}nq^2/m)^{1/2}$ (where $q = \mathbf{1}L$), and the cyclotron frequency $\mathbf{w}_c = qB/mc$ by $\mathbf{x}/\mathbf{a}^2 = 2\mathbf{w}_p^2/\mathbf{w}_c^2$, which is the familiar self-field parameter. As shown in Fig. 5, the maximum of the self-field parameter occurs at $|\hat{P}_q| = 0$, and the maximum value is $2\mathbf{w}_p^2/\mathbf{w}_c^2 = 1$. Therefore, the criterion for the confinement is:

$$2\mathbf{w}_p^2/\mathbf{w}_c^2 \leq 1. \quad (31)$$

Note that $\mathbf{w}_p^2 = \mathbf{w}_c^2/2$ corresponds to the Brillouin density limit^{3, 4}.

B. Confinement for the 3-D System

For the 3-D system when $\hat{P}_q = 0$, we can expand (21) near $\hat{r} = 0$ and find that the lowest order non-constant term, the quadratic term, will be positive when

$$1 - \mathbf{x}/\mathbf{a}^2 - \mathbf{x} \sum_{n=1}^{\infty} n^2 \frac{|K_0(na)|}{|I_0(na)|} + \frac{|K_1(na)|}{|I_1(na)|} \geq 0. \quad (32)$$

By utilizing a formula related to the Wronskian, $I_m(z)K_{m+1}(z) + I_{m+1}(z)K_m(z) = 1/z$, we can simplify (32) to

$$\mathbf{x} \leq \frac{\mathbf{a}^2}{1 + \sum_{n=1}^{\infty} \frac{n\mathbf{a}}{|I_0(na)| |I_1(na)|}}. \quad (33)$$

The upper bound on the self-field parameter for the 3-D system also occurs at

$|\hat{P}_q| = 0$; hence, the criterion for confinement is

$$\frac{2\mathbf{w}_p^2}{\mathbf{w}_c^2} \leq \frac{1}{1 + \sum_{n=1}^{\infty} \frac{n\mathbf{a}}{|I_0(na)| |I_1(na)|}}. \quad (34)$$

Fig. 5 illustrates a few of the critical transition curves in a normalized P_q and $2\mathbf{w}_p^2/\mathbf{w}_c^2$ space. In obtaining the results in Fig. 5, we use Newton's method to simultaneously solve the equations, $F'(\hat{r}) = F''(\hat{r}) = 0$ for fixed values of \hat{r} and \mathbf{a} . Seed values are given to \mathbf{x} and \hat{P}_q , and convergence of these values typically occurs within five iterations. Because the 2-D system corresponds to the limit $a/L \rightarrow \infty$ as discussed in Sec. III, the transition curve for $a/L = \infty$ is identical to the results predicted by (30).

Fig. 6 shows a plot of the upper bounds for transition to occur in the 2-D and 3-D systems. The upper bounds are precisely the intersections of the curves in Fig. 5 with the $P_q = 0$ axis.

Before concluding this section, we consider the following two limits of (34).

Expanding (34) in the limit $\mathbf{a} \gg 1$ (i.e. a nearly unbunched beam) and

$I_0(\mathbf{a}) \approx I_1(\mathbf{a}) \approx e^{na} / (2pna)^{1/2}$, we obtain:

$$\frac{2w_p^2}{w_c^2} \cong 1 - 2pa^2 e^{-2a} = 1 - \frac{8p^3 a^2}{L^2} e^{-4pa/L} \quad (35)$$

which shows that the system asymptotically approaches the 2-D system's Brillouin flow limit for large a/L . The other important limit of (34), $\mathbf{a} \ll 1$ (i.e. a strongly bunched beam), may be solved numerically, and yields:

$$\frac{2w_p^2}{w_c^2} \cong \frac{\mathbf{a}}{p} = \frac{2a}{L} \quad (36)$$

which is significantly lower than the Brillouin density limit.

V. Discussions

We have ignored the realistic effect of a finite bunch size in our present model. Incorporating such an effect would reduce the stringent beam confinement criterion placed on the self-field parameter. Qualitatively, both the beam space charge and the induced surface charges would be less dense, and therefore the beam would experience a reduced electric field force from the conducting wall and the other bunches.

A separate effect for a finite charge bunch would be the evolution of the bunch shape. In order to evaluate the importance of such an effect relative to the beam loss mechanism just described, it is necessary to compare their time scales. We will now give an order of magnitude estimate for the escape time (i.e. the time needed for a particle to escape to the wall).

For simplicity, assume that the particle has no canonical angular momentum ($\hat{P}_q = 0$), and the particle is initially at the center of the conductor ($\hat{r} = 0$). We will assume that the initial radial momentum is nonzero, but relatively small ($0 < \hat{P}_{r0}^2 < \mathbf{a}^2 \ll \mathbf{x}$). Using (17) and ignoring the 3-D correction terms $F(\hat{r})$ we obtain,

$$\mathbf{t} = \int_0^{\mathbf{a}} \frac{d\hat{r}}{\hat{P}_r} = \int_0^1 \frac{d\mathbf{c}}{\left[\hat{P}_{r0}^2 / \mathbf{a}^2 - \mathbf{c}^2 - \mathbf{x} / \mathbf{a}^2 \ln(1 - \mathbf{c}^2) \right]^{1/2}} \quad (37)$$

where $\mathbf{c} = \hat{r} / \mathbf{a}$. Therefore, the escape time is $t = \mathbf{t} / \mathbf{w}_L \sim (\mathbf{x} / \mathbf{a}^2)^{-1/2} / \mathbf{w}_L \sim \mathbf{w}_p^{-1}$.

We can obtain an order of magnitude for the evolution time, by considering the dynamics of only one uniform spherical bunch of radius, R , charge, q , and mass, m , with no conductor present. Using Coulomb's Law and the Lorentz Force Law, we find that

$$\frac{d^2 R}{dt^2} = \frac{q^2}{mR^2}. \quad (38)$$

Equation (38) implies that the evolution time scale is of the order $(mR^3/q^2)^{1/2}$. Assuming the density is of the order $(4pR^3/3)^{-1}$, then the evolution time is of the order w_p^{-1} . Hence, the effect of the bunch shape evolution is, in general, not negligible compared to the beam loss mechanism. Therefore, a detailed investigation of the effect of finite bunch size is required to quantify the confinement of moderately bunched beams.

VI. Summary

In the present paper, we have derived confinement criteria for a highly bunched beam and an unbunched beam propagating down a perfectly conducting cylinder with an applied magnetic field. We have modeled these two systems by approximating the unbunched beam as a rod of charge and the bunched beam as collinear periodic charges. For these two models, we have derived the equations of transverse motion from the Hamiltonian.

The criteria have been obtained by examining the properties of the beam's radial phase space. There are two possible phase spaces, one which allows trapped particle orbits and one which does not. The difference between the two is shown to be caused by the behavior of an effective radial potential (i.e. whether it has a kink or not). When varying the three parameters $\{\mathbf{a}, \mathbf{x}, \hat{P}_q\}$ in the system, the behavior of the effective potential undergoes a critical transition.

The values of $\{\mathbf{a}, \mathbf{x}, \hat{P}_q\}$ where the critical transition occurs yield an upper bound on the self-field parameter $2\mathbf{w}_p^2/\mathbf{w}_c^2 \equiv \mathbf{x}/\mathbf{a}^2$ for which trapped particle orbits exists. For an unbunched beam, the upper bound on the self- field parameter has been shown to be $2\mathbf{w}_p^2/\mathbf{w}_c^2 \leq 1$, which is precisely the Brillouin density limit. For a bunched beam, the maximum value of the self-field parameter is given in (34). The limit on the self-field parameter will always be less for the bunched beam than for the unbunched beam due to the higher local density of internal charges and induced surface charges, which contribute a higher electric field force.

The results reported in this paper are applicable to a relativistic charged-particle beam by a proper application of the Lorentz transformation from the laboratory frame to the frame of reference moving with the beam. Finally, it is anticipated that the results in this paper will provide a useful insight into the confinement of high-intensity bunched beams in linear accelerators as well as in high-power microwave sources such as klystrons.

Appendix. Calculation of the Electrostatic Self - Field

When calculating the self-field force, we may assume that $\mathbf{q}' = \hat{z}' = 0$, without loss of generality, and express $\vec{r}' = \frac{L}{2p} \hat{r}' \hat{e}_{x'}$, and $\vec{r}_s = \frac{La \cos q}{2p} \hat{e}_x + \frac{La \sin q}{2p} \hat{e}_y + \frac{L\hat{z}}{2p} \hat{e}_z$. Since $E_z \cdot \vec{r}' = E_q \cdot \vec{r}' = 0$ by the symmetries of the system in the longitudinal and azimuthal directions, we need only consider the force along the direction of $\hat{e}_{r'} = \hat{e}_{x'}$. Making use of the expressions,

$$\frac{(\vec{r}' - \vec{r}_s) \cdot \hat{x}}{|\vec{r}' - \vec{r}_s|^3} = -\frac{\left(\frac{2p}{aL}\right)^2 \cos q - \frac{\hat{r}'}{a}}{\left|1 + \frac{\hat{r}'^2}{a^2} + \frac{\hat{z}^2}{a^2} - 2\frac{\hat{r}'}{a} \cos q\right|^{3/2}}.$$

and $dS = a dz dq = \left(\frac{L}{2p}\right)^2 a d\hat{z} dq$, we may express (12) as

$$E^{self} = -4 \int_0^{\tilde{h}} d\mathbf{h} \int_0^{\tilde{h}} \frac{(\cos q - \mathbf{b}) s dq}{\left|1 + \mathbf{b}^2 + \mathbf{h}^2 - 2\mathbf{b} \cos q\right|^{3/2}} \quad (\text{A1})$$

where $\mathbf{h} = \hat{z}/a$ and $\mathbf{b} = \hat{r}'/a$, and we have also used the longitudinal and azimuthal symmetries to change the limits of integration.

Substituting (10) into (A1), we find that the self-electric field produced by the 2-D induced surface charge at the line charge is

$$\begin{aligned} E_{2D}^{self} &= \frac{4(1 - \mathbf{b}^2)l}{La} \int_0^{\tilde{h}} \frac{dq (\cos q - \mathbf{b})}{\left|1 + \mathbf{b}^2 - 2\mathbf{b} \cos q\right|} \int_0^{\tilde{h}} \frac{d\mathbf{h}}{\left|1 + \mathbf{b}^2 + \mathbf{h}^2 - 2\mathbf{b} \cos q\right|^{3/2}} \\ &= \frac{4pl}{L} \frac{\hat{r}'}{a^2 - \hat{r}'^2} \end{aligned} \quad (\text{A2})$$

which is identical to (13). This result can also be obtained easily using the method of images.¹³

Of course, the first term in (14) corresponds to the 2-D component, which we have just derived. Substituting (11) into (A1), we can express the self-electric field produced by the 3-D induced surface charge at the point charge as,

$$E_{3D}^{self} = \frac{4pq}{L^2} \left[\frac{\hat{r}'}{a^2 - \hat{r}'^2} \right] + \frac{8q}{aL^2} \sum_{n=1}^{\infty} \frac{I_0 \hat{r}'^n \Theta_{n0}}{I_0 \hat{r}'^n} + \frac{16q}{aL^2} \sum_{n=1}^{\infty} \sum_{l=1}^{\infty} \frac{I_l \hat{r}'^n \Theta_{nl}}{I_l \hat{r}'^n} \quad (A3)$$

where

$$\begin{aligned} \Theta_{nl} &= \int_0^{\pi} \int_0^{\pi} \frac{\cos(nah) \cos(lq) \cos q - b}{(1 + b^2 + h^2 - 2b \cos q)^{3/2}} dh dq \\ &= \frac{\partial}{\partial b} \int_0^{\pi} \int_0^{\pi} \frac{\cos(nah) \cos(lq)}{(1 + b^2 + h^2 - 2b \cos q)^{1/2}} dh dq \\ &= \frac{\partial}{\partial b} \int_0^{\pi} \left[K_0 \left(\frac{a}{\sqrt{1 + b^2 - 2b \cos q}} \right) \cos(lq) \right] dq \\ &= \frac{\partial}{\partial b} \int_0^{\pi} \left[I_0 \left(\frac{a}{b} \right) K_0 \left(\frac{b}{a} \right) + 2 \sum_{p=1}^{\infty} I_p \left(\frac{a}{b} \right) K_p \left(\frac{b}{a} \right) \cos(pq) \right] \cos(lq) dq \\ &= p K_l \left(\frac{a}{b} \right) \frac{\partial}{\partial b} I_l \left(\frac{a}{b} \right) \\ &= p n a K_l \left(\frac{a}{b} \right) I_l \left(\frac{a}{b} \right) \end{aligned} \quad (A4)$$

In the third step in (A4), we made use of the relation¹⁴,

$$\int_0^{\pi} \frac{\cos(ax) dx}{\sqrt{b^2 + x^2}} = K_0 \left(\frac{a}{b} \right),$$

while in step 4 we used the formula¹⁵,

$$K_0 \left(\frac{a}{\sqrt{a^2 + b^2 - 2ab \cos q}} \right) = I_0 \left(\frac{a}{b} \right) K_0 \left(\frac{b}{a} \right) + 2 \sum_{p=1}^{\infty} I_p \left(\frac{a}{b} \right) K_p \left(\frac{b}{a} \right) \cos(pq), \quad 0 \leq a < b.$$

Substituting (A4) into (A3) yields (14).

Acknowledgement

This work was supported by the Air Force Office of Scientific Research, Grant No. F49620-97-1-0480 and Grant No. F49620-00-1-0007, and by the Department of Energy, Office of High Energy and Nuclear Physics, Grant No. DE-FG02-95ER-40919

References

- ¹R. C. Davidson, *Physics of Nonneutral Plasmas* (Addison-Wesley, Reading, Massachusetts, 1990).
- ²M. Reiser, *Theory and Design of Charged Particle Beams* (John Wiley & Sons, New York, 1994).
- ³L. Brillouin, *Phys. Rev.* **67**, 260 (1945).
- ⁴See, for example, Chap. 1 and p. 545 of Ref. 1.
- ⁵F. J. Sacherer, *IEEE Trans. Nucl. Sci.* NS-18, 1105 (1971).
- ⁶J. J. Barnard and S. M. Lund, in *Proceedings of the Particle Accelerator Conference*, edited by M. Comyn (Institute of Electrical and Electronics Engineers, Piscataway, NJ, 1997), p. 1929.
- ⁷R. L. Gluckstern, A. V. Fedotov, S. Kurennoy, and R. Ryne, *Phys. Rev. E* **58**, 4977 (1998).
- ⁸C. Chen and R. Pakter, *Phys. Plasmas* **5**, 2203 (2000).
- ⁹C. Chen and R. Pakter, "Electron Beam Halo Formation in High-Power Klystron Amplifiers," *IEEE Trans. Plasma Sci.*, in press (2000).
- ¹⁰C. Chen and R. Pakter, "Halo Formation in Intense Electron Beams in High-Power Klystron Amplifiers," in *Intense Microwave Pulses VI*, edited by H. E. Brandt, *SPIE Proc.* 3702, 21 (1999).
- ¹¹J. D. Jackson, *Classical Electrodynamics*, 2nd ed. (John Wiley & Sons, New York, 1975), Ch. 3.
- ¹²M. Hess, R. Pakter, and C. Chen, "Green's function description of space charge in intense charged-particle beams," *Proceedings of the Particle Accelerator Conference*,

edited by A. Luccio and W. Mackay (Institute of Electrical and Electronics Engineers, Piscataway, NJ, 1999), p. 2752.

¹³G. Barton, *Elements of Green's Functions and Propagation* (Oxford University Press Inc., New York, 1995), p. 412-416.

¹⁴I. S. Gradshteyn and I. M. Ryzhik, *Table of Integrals, Series, and Products*, 5th ed. (Academic Press, London, 1994), p. 464.

¹⁵A. Gray and G. B. Mathews, *A Treatise on Bessel Functions and Their Applications to Physics*, 2nd ed. (MacMillan and Co., London, 1952), p. 74.

Figure Captions

- Fig. 1. Schematics of (a) line charge and (b) periodic array of charges in a perfectly conducting cylinder.
- Fig. 2. Plots of the effective potential $F(\hat{r})$ vs. \hat{r} in the 2-D system for the choices of system parameters corresponding to: (a) $\mathbf{x}/\mathbf{a}^2 = 0.5$ and $\hat{P}_q/\mathbf{a}^2 = 0.01$, and (b) $\mathbf{x}/\mathbf{a}^2 = 3.0$ and $\hat{P}_q/\mathbf{a}^2 = 0.01$.
- Fig. 3. Plots of the radial phase space in the 2-D system for the two cases with the same choices of the system parameters as those shown in Figs. 2(a) and 2(b).
- Fig. 4. Plots of the radial phase space in the 3-D system for the choices of system parameters corresponding to: (a) $\mathbf{x}/\mathbf{a}^2 = 0.5$, $\hat{P}_q/\mathbf{a}^2 = 0.01$ and $\mathbf{a} = 1.0$, and (b) $\mathbf{x}/\mathbf{a}^2 = 0.1$, $\hat{P}_q/\mathbf{a}^2 = 0.01$ and $\mathbf{a} = 1.0$.
- Fig. 5. Plots of the maximum value of the self-field parameter $2\mathbf{w}_p^2/\mathbf{w}_c^2$ for confinement as a function of normalized canonical angular momentum $2P_q/m\mathbf{w}_c a^2$ for several values of the aspect ratio a/L in the 3-D system. Note that the 2-D system corresponds to the limit $a/L = \infty$, and the curve with $a/L = \infty$ is obtained from (30).
- Fig. 6. Plots of the maximum value of the self-field parameter $2\mathbf{w}_p^2/\mathbf{w}_c^2$ for confinement as a function of the aspect ratio a/L for $P_q = 0$ in both the 2-D and 3-D systems.

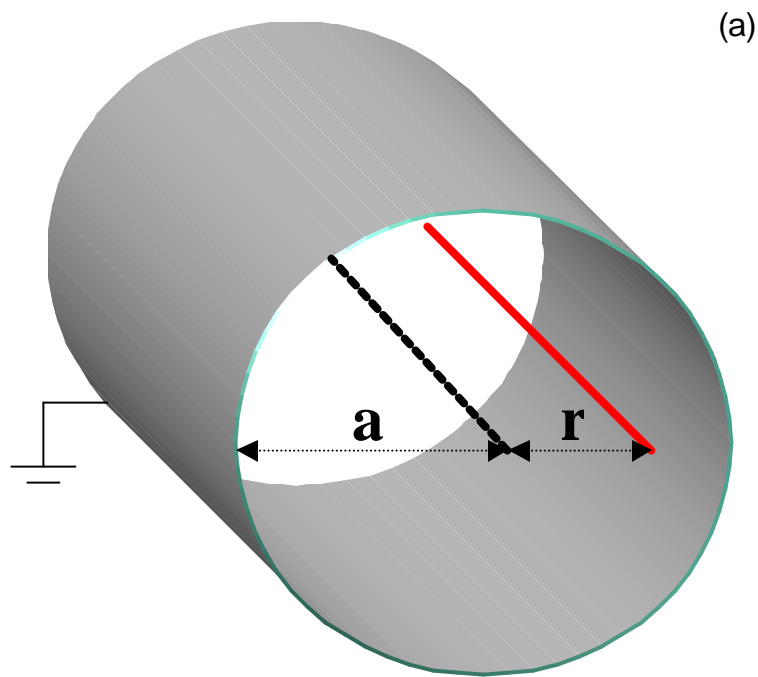


Fig. 1(a)

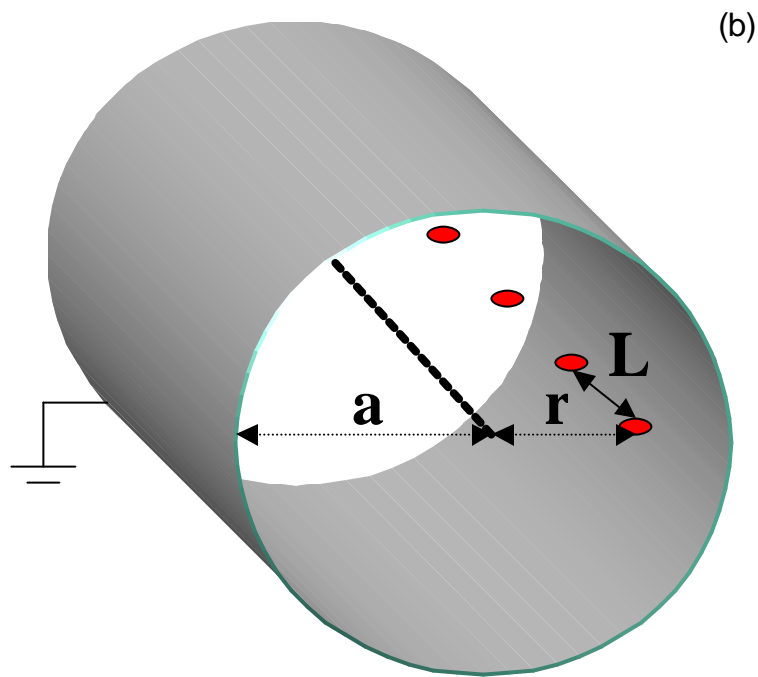


Fig. 1(b)

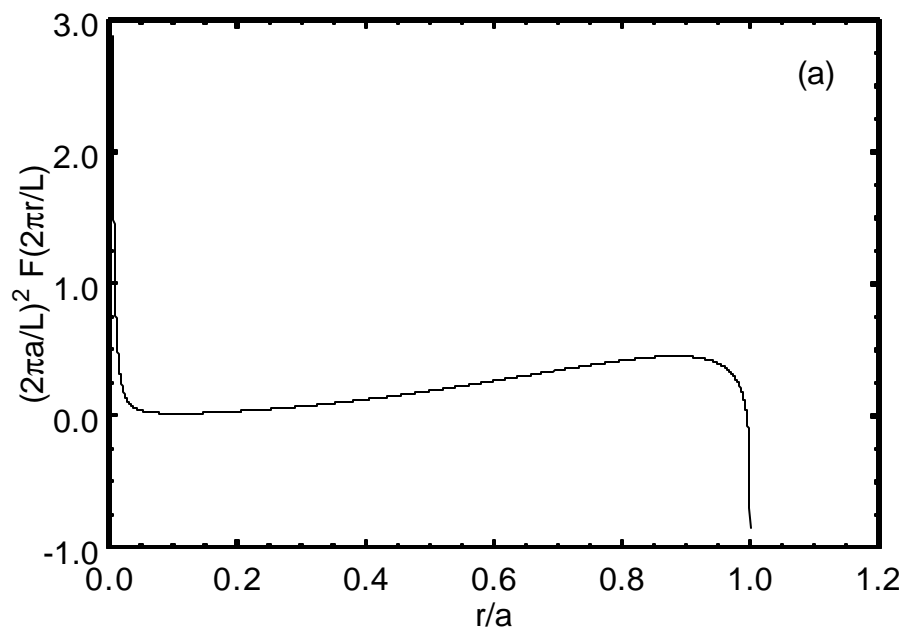


Fig. 2(a)

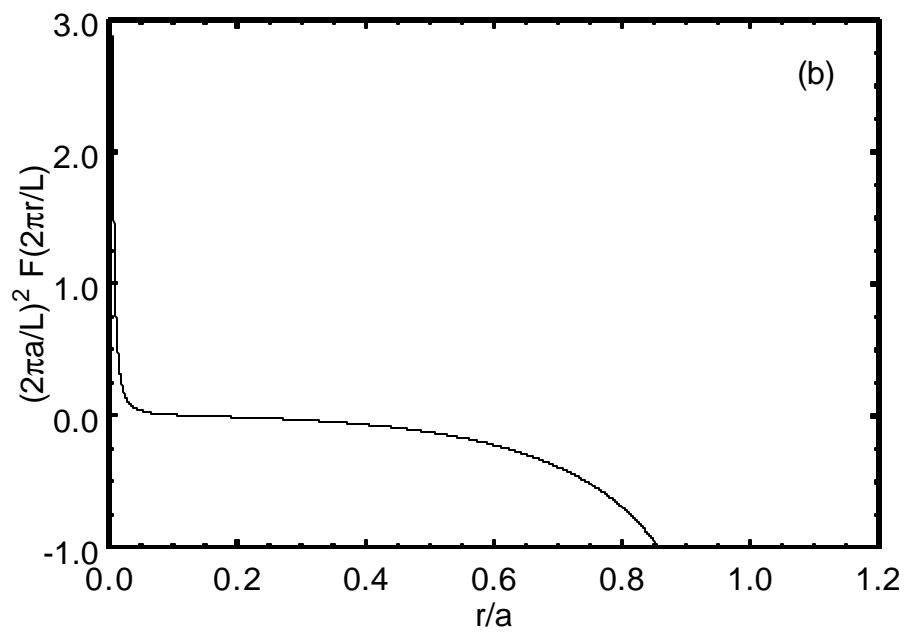


Fig. 2(b)

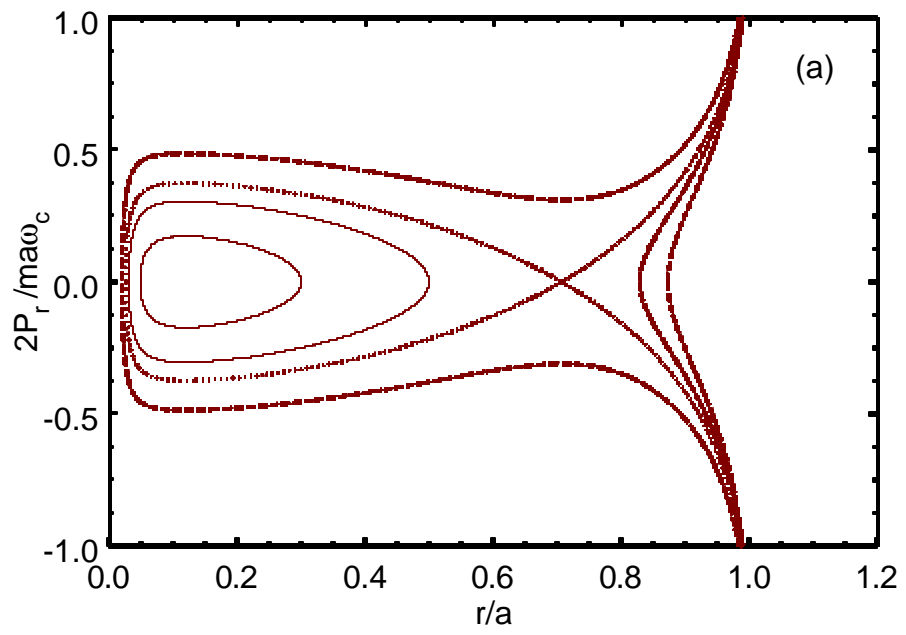


Fig. 3(a)

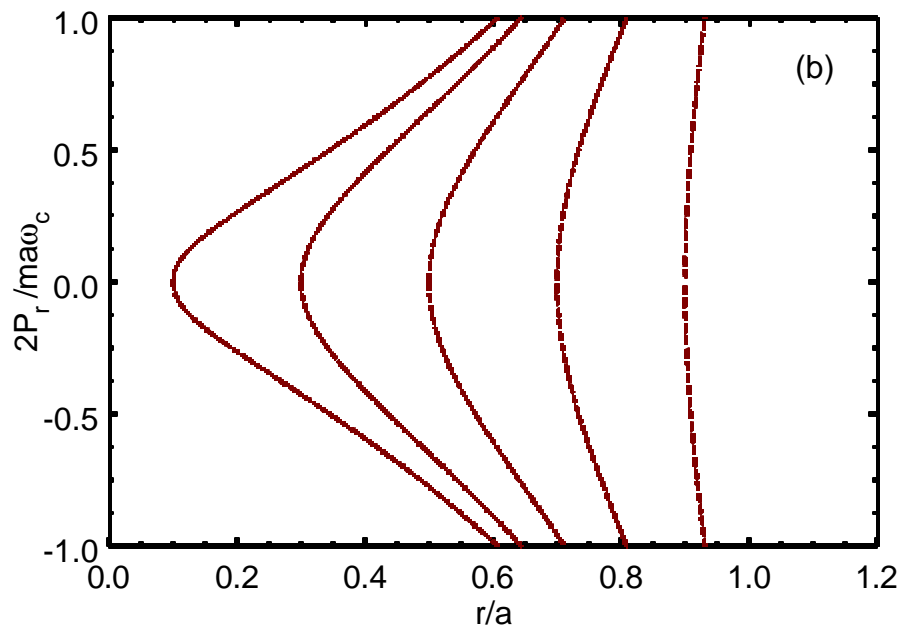


Fig. 3(b)

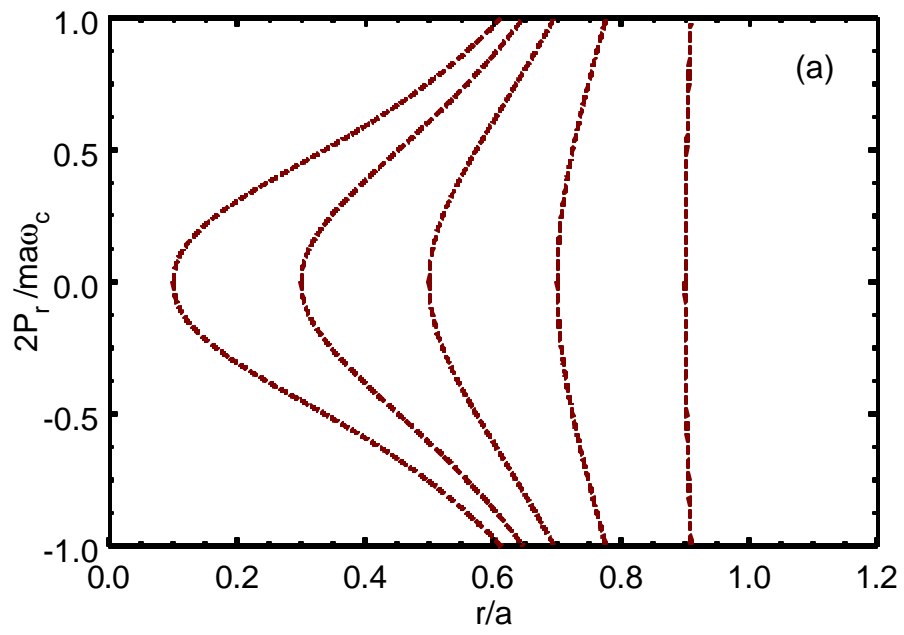


Fig. 4(a)

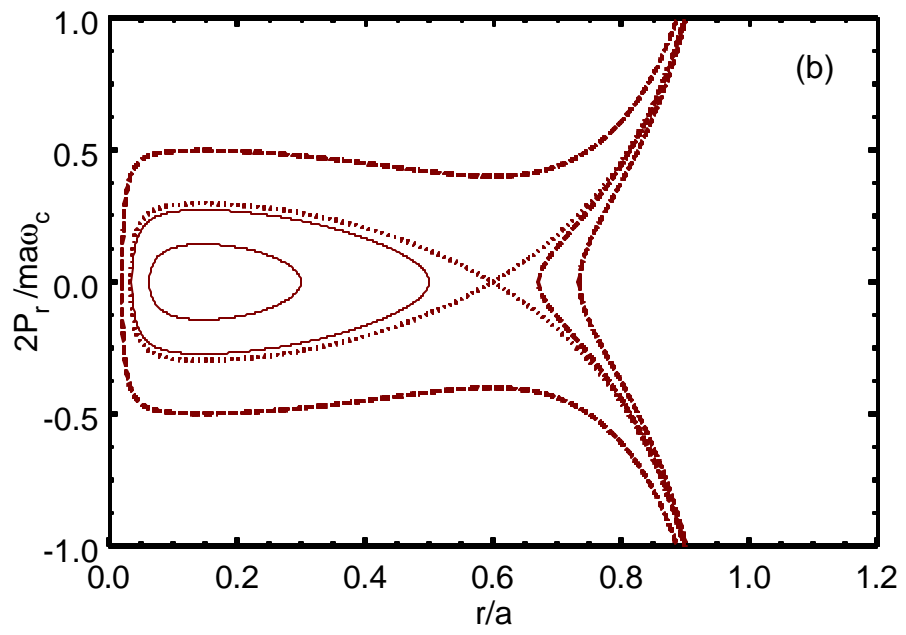


Fig. 4(b)

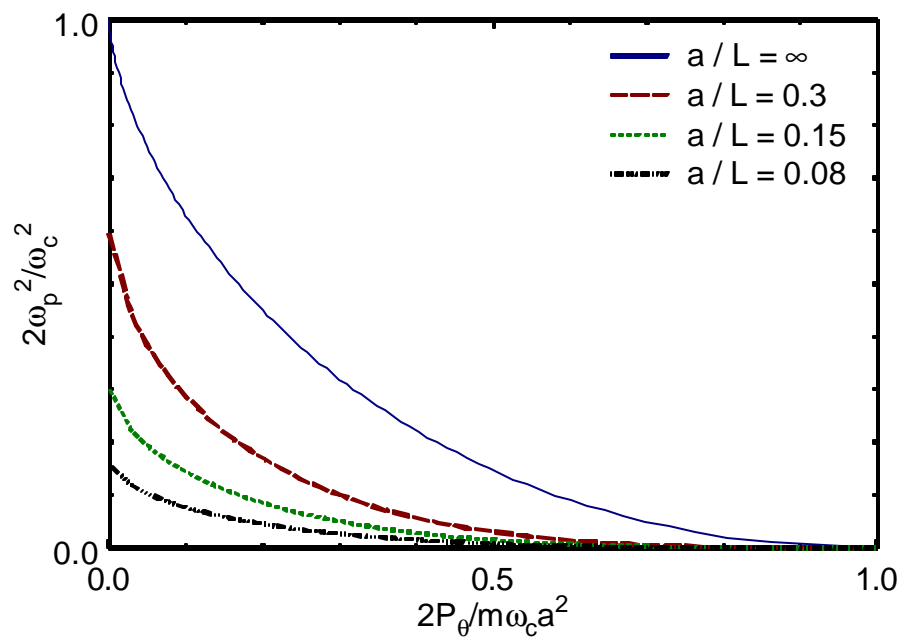


Fig. 5

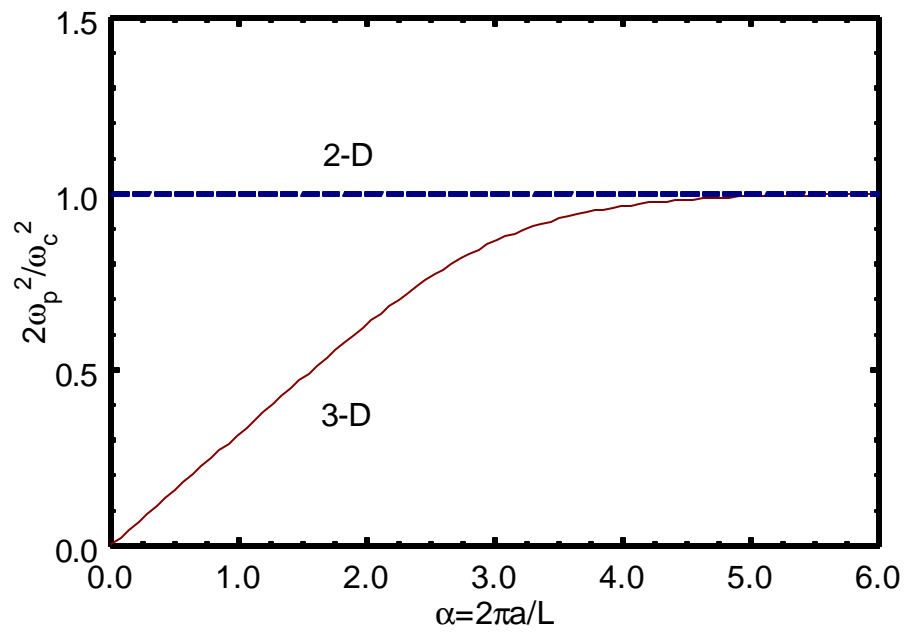


Fig. 6